scientific reports

Check for updates

OPEN

Kinetic interplay between droplet maturation and coalescence modulates shape of aged protein condensates

Adiran Garaizar[1,2,4], Jorge R. Espinosa[1,2,4], Jerelle A. Joseph[1,2,3] & Rosana Collepardo-Guevara[1,2,3]✉

Biomolecular condensates formed by the process of liquid–liquid phase separation (LLPS) play diverse roles inside cells, from spatiotemporal compartmentalisation to speeding up chemical reactions. Upon maturation, the liquid-like properties of condensates, which underpin their functions, are gradually lost, eventually giving rise to solid-like states with potential pathological implications. Enhancement of inter-protein interactions is one of the main mechanisms suggested to trigger the formation of solid-like condensates. To gain a molecular-level understanding of how the accumulation of stronger interactions among proteins inside condensates affect the kinetic and thermodynamic properties of biomolecular condensates, and their shapes over time, we develop a tailored coarse-grained model of proteins that transition from establishing weak to stronger inter-protein interactions inside condensates. Our simulations reveal that the fast accumulation of strongly binding proteins during the nucleation and growth stages of condensate formation results in aspherical solid-like condensates. In contrast, when strong inter-protein interactions appear only after the equilibrium condensate has been formed, or when they accumulate slowly over time with respect to the time needed for droplets to fuse and grow, spherical solid-like droplets emerge. By conducting atomistic potential-of-mean-force simulations of NUP-98 peptides—prone to forming inter-protein β-sheets—we observe that formation of inter-peptide β-sheets increases the strength of the interactions consistently with the loss of liquid-like condensate properties we observe at the coarse-grained level. Overall, our work aids in elucidating fundamental molecular, kinetic, and thermodynamic mechanisms linking the rate of change in protein interaction strength to condensate shape and maturation during ageing.

Living cells contain numerous macromolecular components, which must be organised in space and time to facilitate the concerted regulation of biochemical reactions[1–4]. In eukaryotes, such functional organisation is achieved via the formation of both membrane-bound[5] and membrane-less compartments[2,6]. The latter, also termed biomolecular condensates[7], are liquid drops of varying compositions thought to form via liquid–liquid phase separation (LLPS) when a critical concentration of key multivalent biomolecules (such as proteins and RNA) is surpassed[2,6]. Biomolecular condensates are ubiquitous within both the cytoplasm[8] and nucleoplasm[9–12]; with the most well-known examples including P granules[13], nucleoli[14–19], Cajal bodies[20–22], or stress granules[23]. Biomolecular condensates have also been identified as functional organisers of the interiors of prokaryotes[24].

Intracellular LLPS is a delicate phenomenon which is sensitively affected by the environmental conditions (e.g., pH, salt, and temperature)[25,26], and the presence of different molecular partners[15,27,28]. Alteration of such conditions can lead to misregulation with pathological implications[29–31]. Indeed, the gradual rigidification of biomolecular condensates with time (also known as 'maturation' or 'ageing') has been associated to the proliferation of multiple neurodegenerative diseases[29–33]—such as amyotrophic lateral sclerosis (ALS)[34], Parkinson's[35], Alzheimer's[36], and frontotemporal dementia (FTD)—and of certain types of cancers[37] and diabetes[38]. Therefore, understanding the molecular mechanisms influencing aberrant LLPS is a key area of biomedical research[39].

[1]Maxwell Centre, Cavendish Laboratory, Department of Physics, University of Cambridge, J J Thomson Avenue, Cambridge CB3 0HE, UK. [2]Yusuf Hamied Department of Chemistry, University of Cambridge, Lensfield Road, Cambridge CB2 1EW, UK. [3]Department of Genetics, University of Cambridge, Downing Site, Cambridge CB2 3EH, UK. [4]These authors contributed equally: Adiran Garaizar and Jorge R. Espinosa. ✉email: rc597@cam.ac.uk

Macroscopically, biomolecular condensates present liquid-like properties, such as the ability to coalesce and deform under shear flow[13], exhibit spherical shapes[2,29,40], show short recovery times from fluorescence recovery after photobleaching (FRAP) or GFP florescence recovery experiments[22,34,36], and exchange material rapidly with their environment[41]. Microscopically, such liquid-like properties originate on the weak multivalent attractive interactions that the biomolecules within the condensate establish. Weak interactions translate into dynamic binding and unbinding, free molecular diffusion within, and facile exchange of species in and out of condensates. Overall, the liquid-like behaviour of molecules enables condensates to fulfill a wide-range of biological functions, from acting as curated reactive volumes that selectively concentrate and exclude specific molecules[4], buffering of protein concentrations[42], regulating gene expression[10,43–45], sensing changes in the cell environment[46], to sequestering components harmful in the cell[47].

Although the liquid-like properties of condensates seem to underpin their functions during health, it is now clear that the material properties of condensates extend far beyond those of low viscous liquids[39,48]. Indeed, condensates encompass low to high viscosity fluids[49,50], hydrogels[51,52] and solid-like states[53,54]. These properties are not surprising if one considers that the physicochemical features of the biomolecules known to form condensates are highly heterogeneous too. These include multidomain proteins, instrinsically disordered regions (IDRs), and globular proteins with different chemical makeups[2,55], and which can undergo LLPS in pure form via homotypic interactions and/or in partnership with other proteins[15,56,57], RNAs[58–60], DNA[9,10,61], or chromatin[62–64] via heterotypic interactions. Furthermore, FRAP, GFP florescence recovery, coalesence, and active and passive microrheology experiments have revealed that over time, even the condensates that are originally liquid-like can transition to gels or soft glasses upon maturation[23,34,49,65]. Matured condensates display reduced fusion propensities and longer recovery times after photobleaching[7,29,34,35,65–69], which suggest that the diffusion of molecules within is significantly reduced. Several factors have been proposed as key drivers for the liquid-to-solid transition of condensates, including altered salt-concentration or temperature[49,70], post-translational modifications[36,71], protein mutations[34,72,73], and protein folding and misfolding events[74–79]. All these factors are expected to favour rigidification by increasing the binding affinity among species and slowing down the timescales of inter-protein unbinding events.

In this work, we develop a coarse-grained (CG) simulation approach to investigate the impact of the gradual strengthening of inter-protein interactions—due for instance to the accumulation of inter-protein β-sheets[74–76,79,80], post-translational modifications[81], or changes in the condensate microenvironment[26]—in the kinetics and stability of protein condensates over time. Our CG simulations reveal that the interplay of the timescales of condensate growth and fusion, and the rate of emergence of stronger inter-protein interactions, critically dictates condensate shape: with spherical condensates forming when fusion dominates, and aspherical solid-like states arising when the stronger interactions accumulate faster than the timescales of condensate fusion. Finally, using atomistic simulations, we show that formation of inter-protein β-sheets can strengthen interactions sufficiently to trigger the type of dynamical arrest of condensates we observe at the coarse-grained level. Taken together, our simulations provide a time-dependent assessment of the modulation of the dynamic properties of proteins inside condensates, and contrast kinetics and thermodynamics properties of condensates sustained by strong versus transient inter-protein interactions.

Results and discussion

Strengthening of inter-protein interactions can cause condensate maturation and thermal hysteresis. We begin by investigating how strengthening of inter-protein interactions affects the thermodynamic and rheological properties of condensates. For this purpose, we develop a tailored coarse-grained model that can assess the impact of transient versus long-lived protein binding on the kinetic and thermodynamic properties of the condensates they form. Our model approximates an intrinsically disordered protein as a fully flexible Lennard-Jones heteropolymer of beads connected by harmonic springs (see Fig. 1A, and section *SIA* of the Supplementary Information (SI)). Each bead represents a protein binding region that corresponds to a linearly consecutive group of around six to eight amino acids. Such bead resolution is arbitrarily defined to represent the smallest protein regions that undergo disorder-to-order transitions[74], or that can accumulate sufficient post-transnational modifications or mutations to result in significant strengthening of inter-protein interactions. We set each heteropolymer to contain 39 beads, or 234–312 amino acids, which is well within the typical length of many insitrinsically disorder protein regions of intracellular phase separating proteins (e.g. hnRNPA1 IDR, FUS PLD, LAF-1 IDR, DDX4 N-terminal domain). Within a single heteropolymer, we combine beads representing two different types of 'sticker' regions (labelled A and B beads) prone to establishing strong heterotypic interactions with their complementary stickers (i.e., A–B pairs), and beads representing 'spacer' regions that only establish weak interactions (Fig. 1A). Specifically, we distinguish two types of possible interactions among beads: (1) weak interactions for any sticker–spacer and spacer–spacer pair, and for homotypic sticker–sticker pairs. Pairs of weakly (i.e., interactionstrength equal to ε_D), and (2) strengthened interactions only among complementary pairs of 'sticker A–sticker B' beads (i.e., 10 times stronger or equal to $\varepsilon_S = 10\varepsilon_D$) (Fig. 1A). The latter restriction of only considering strong interactions among pairs of complementary A–B stickers, rather than among all stickers, is set to implicitly consider that stronger interactions would most likely be favoured among sticker regions that are not only in spatial proximity but also favourably orientated with respect to one another. The stickers-vs-spacers sequence patterning of vs. weak) of our coarse-grained proteins is shown in Figs. 1A and S1A (Top). Moreover, an alternative patterning for strong versus weak interactions in which beads representing sticker domains are only located along the first half of the coarse-grained sequence (Fig. S1A (Bottom)) is also explored in the *SI* to elucidate possible patterning effects in condensate maturation. The comprehensive description of the coarse-grained potentials and a full list of the model parameters, as well as protein sequences and the employed reduced units are provided in Sections *SIA* and *SIB* of the Supplementary Information.

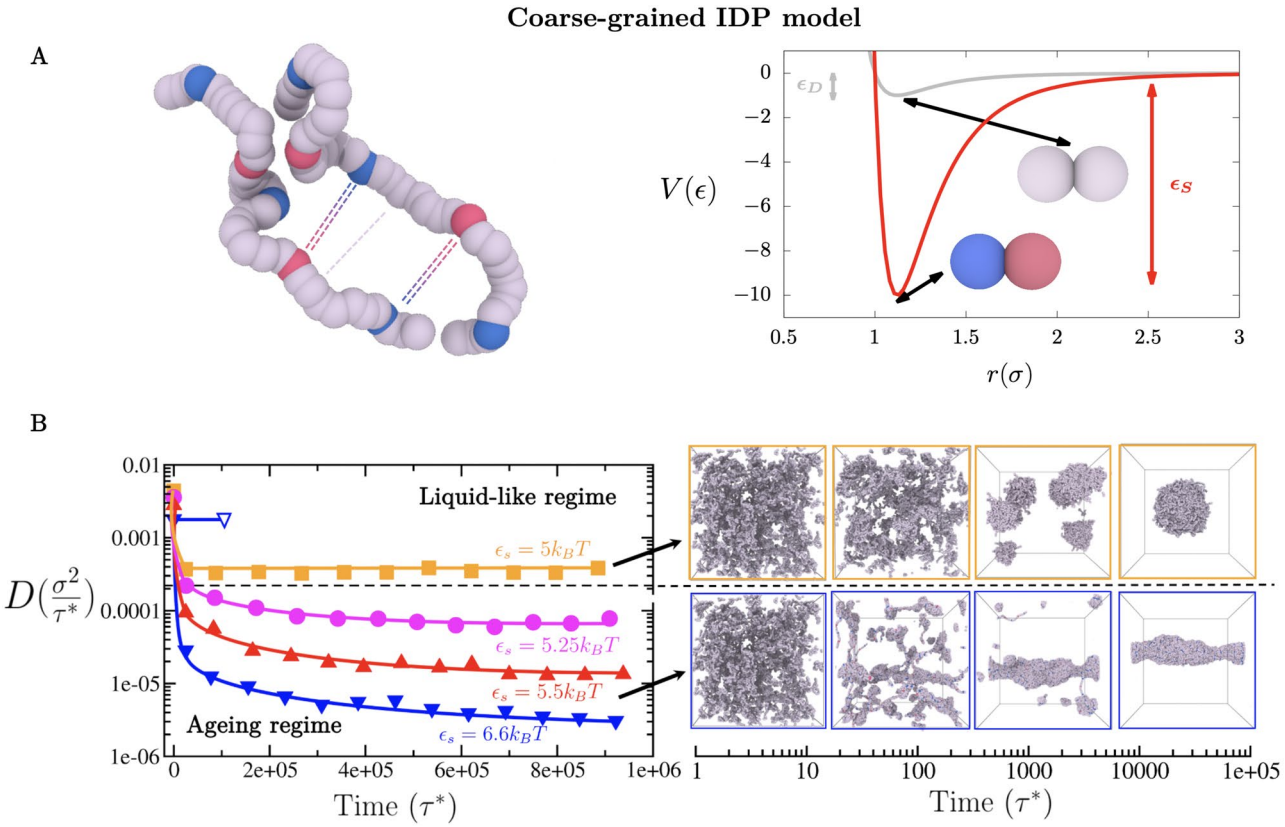

Figure 1. (**A**) Coarse-grained representation of intrinsically disordered proteins composed of stickers of type A (depicted as blue beads), stickers of type B (depicted as red beads), and spacers (depicted as grey beads). The model considers transient weak interactions among spacer–spacer, spacer–sticker, and homotypic sticker–sticker pairs (i.e., sticker A–sticker A and sticker B–sticker B pairs; grey curve), and strong longer-lived interactions among heterotypic sticker A–sticker B pairs (red curve). A Lennard-Jones potential of different well-depths is used to represent the associative interactions among the different types of beads: ε_D is used for interactions between weakly binding bead pairs, and ε_S for interactions between strongly binding 'sticker A–sticker B' bead pairs. Each bead represents a group of $\sim$ 6–8 amino acids. Each protein is composed of 39 beads: 3 blue beads, 2 red beads and 34 grey ones. The excluded volume (σ) of each segment type is the same. Results for an alternative CG representation of strong protein binding and a different protein sequence patterning to that depicted in (**A**) are available in the Supplementary Information. (**B**) Time-evolution of the protein diffusion coefficient (D) in the condensed phase for different interaction strengths ε_S (in k_BT) between strongly-binding protein segments (please note that $\varepsilon_S = 10\varepsilon_D$). The horizontal black dashed line represents the kinetic threshold of our simulation timescale that distinguishes between ergodic liquid-like behaviour and ageing (transient liquid-to-solid) behaviour. Interaction strengths lower than $5.25k_B$T between the strongly-binding segments permit liquid-like behaviour (up to $\varepsilon_S = 3.5k_B$T and $\varepsilon_D = 0.35k_B$T where LLPS is no longer possible), while equal or higher strengths lead to the gradual deceleration of protein mobility over time as shown by D. However, in absence of strongly-binding segments (i.e., where all beads bind to one another with uniformly weak binding strength), liquid-like behaviour can be still observed even at ε_D values of $0.66k_B$T (empty blue triangle). Black arrows indicate the time dependent behaviour of condensates over time in the liquid-like (Top) and ageing regimes (Bottom). The time evolution snapshots of the condensate corresponds to systems with $\varepsilon_S = 5k_B$T (Top) and $\varepsilon_S = 6.6k_B$T (Bottom). Please note that these snapshots do not correspond to the NVT bulk systems employed to compute the diffusion coefficient in the B left panel.

As a control, we begin by characterising the dynamical properties of proteins inside condensates in the absence of strengthen interactions. In such a homopolymer model, a value of the bead–bead interaction strength, ε_D, larger than 0.35 k_BT enables the formation of phase-separated droplets. Therefore, we perform unbiased Molecular Dynamics (MD) simulations of roughly 730 interacting homopolymers proteins in the *NVT* ensemble, where all beads bind to one another with a uniform binding strength equal to $\varepsilon_D = 0.66\,k_B$T; such value of ε_D is high enough to induce condensate formation. From bulk simulations at the equilibrium condensate density, we estimate the mean square displacement (MSD) of the central bead of each protein (in σ units, the molecular diameter of every bead in our model), and calculate the value of the diffusion coefficient (D) of proteins within the condensates as a function of time (in reduced units τ^*) (Empty blue triangle of Fig. 1B; for further details on these calculations see *SIB* of the Supplementary Information). We observe that the diffusion coefficient of proteins within the droplets quickly converges reaching a value of $\sim\ 0.002\,\sigma^2/\tau^*$, characteristic of the free diffusion of polymers within liquids.

We next investigate the change in the mobility of the proteins within condensates when long-lived binding due to strengthening of inter-protein interactions occurs. To do so, we use our heteropolymer model, where now 34 beads are treated as spacer regions (i.e., bind to one another weakly with ε_D) and 5 beads are treated as sticker regions (i.e., bind to most regions weakly with ε_D, but to complementary sticker regions strongly with ε_S). Note that the value of ε_D controls the strength of interactions among both weakly and strongly binding regions ($\varepsilon_D = \varepsilon_S/10$). Since the strengthening of inter-protein interactions would depend on the sequence of the amino acids involved[79,82] and the physicochemical factors driving such strengthening (e.g. disorder-to-order transitions[74–76,79,80], post-translational modifications[81], or changes in salt conditions[26]), we explore the dependence of the changes in protein diffusion within condensates on the relative binding interaction strength among beads. Given that values of ε_D larger than 0.35 k_BT enable the formation of phase-separated droplets, we vary ε_D from 0.5 to 0.66 k_BT, and ε_S correspondingly (Fig. 1B Left). These tests reveal that when proteins bind to one another weakly ($\varepsilon_D = 0.5\,k_B$T and $\varepsilon_S = 5\,k_B$T, orange curve), the average diffusion coefficient of proteins within the droplets decays moderately due to the emergence of small clusters of strong inter-protein contacts. The diffusion coefficient then quickly plateaus at a sufficiently high value—signalling ergodic liquid-like behaviour. In contrast, at stronger protein interaction strengths ($\varepsilon_S \geq 5.25\,k_B$T, magenta, red and blue curves), the diffusion coefficient decays significantly and now fails to reach a plateau within the explored simulation timescale. Note that to measure D over time, we choose sufficiently large windows of time that allow the central bead of the proteins to diffuse distances at least 3–5 times their molecular diameter; over time, due to the deceleration of the protein mobility, these windows need to be expanded to longer timescales to fulfill the required length scale of sampling. The observed behaviour of the diffusion coefficient signals a significant and continuous decay in the protein mobility, consistent with progressive condensate maturation[23,34,49,65]. Moreover, the emergence of strong binding domains results in a moderate gradual densification of the droplets (Fig. S2). Such condensate densification, as well as the reduction in protein mobility, are driven by the gradual accumulation of strong intermolecular interactions (Fig. S3); this is in contrast to the quick equilibration of the diffusion coefficient in our control simulations, where we treated proteins as weakly-binding homopolymers (even at a value of $\varepsilon_D = 0.66\,k_B$T, blue empty triangle). Decreased mobility of proteins over time, leading to aged condensates (i.e., the 'ageing regime'), has been inferred experimentally from decelerated diffusion coefficients, higher condensate viscosities[35,83], and lower or incomplete recovery from photobleaching[7,29,34,35,65–69,84]. Moreover, from Fig. 1B we can observe how the protein diffusion coefficient within the condensates is highly sensitive to small variations in the binding strength between domains. That is, the diffusion coefficient decreases by several orders of magnitude when the binding strength among domains (ε_S) is raised from 5 to 6.6 k_BT.

Our simulations reveal that there is a clear inter-protein interaction strength threshold that separates ergodic liquid-like behaviour from non-ergodic ageing behaviour towards glassy droplets ($\varepsilon_S > 5\,k_B$T), which we depict by a horizontal black dashed line in Fig. 1B (Left panel). Above such threshold, condensates readily equilibrate and form spherical droplets within the accessible simulation timescales. Below this threshold, condensates gradually become kinetically trapped, forming amorphous droplets due to the emergence of long-lived interactions that hinder the diffusion of proteins within (Fig. 1B Right panel). These independent simulations further support the location of the kinetic threshold shown in Fig. 1B (Left panel). The timescale for the onset of strong binding between protein regions during nucleation and growth of the condensates, significantly impacts condensate shape (Fig. 1B Right panel). As expected, condensates that emerge from proteins that bind to one another weakly (i.e., $\varepsilon_S \leq 5\,k_B$T) grow into spherical liquid droplets. Spherical shapes are favoured because they minimise the surface-to-volume ratio and the interfacial free energy cost within the surrounding dilute phase and under the specific imposed box dimensions and number of protein replicas[85]. However, we note that for other box dimensions with higher global densities, slabs and cylindrical droplets can also minimise the surface-to-volume ratio and the interfacial free energy of the system[86]. Nevertheless, in our box system sizes, the simulations of homopolymers proteins (i.e., where all residues bind to one another evenly) can form both spherical condensates at low to moderate values of the protein–protein binding strength (from $\varepsilon_D > 0.4\,k_B$T to $\varepsilon_D < 0.9\,k_B$T; Fig. S8 (Top panel)) and amorphous kinetically-arrested condensates at higher values ($\varepsilon_D > 1\,k_B$T) (see almost instantaneously quenching in protein diffusivity in Fig. S8 (Bottom panel)). We find that condensates resulting from heteropolymer proteins that contain both weakly binding spacers, and stickers that bind to complementary stickers more strongly (i.e., $\varepsilon_S \geq 5.25\,k_B$T), always give rise to aspherical kinetically-arrested condensates (Fig. 1B Right Bottom panel). In this case, the emergence of longer-lived interactions prevents individual proteins from relaxing and conveniently rearranging within the condensate to minimise the surface tension, and thus, their free energy[87,88]. We also note that a qualitatively similar behaviour is obtained when the strongly interacting sticker beads are placed along the first half of the sequence (Fig. S4) rather than distributed over its full length (Fig. 1B). Only a moderate increase of the inter-protein interaction strength threshold ($\varepsilon_S \geq 6\,k_B$T) respect to that shown in Fig. 1B ($\varepsilon_S \geq 5.25\,k_B$T) is required to switch from ergodic liquid-like behaviour to transient ageing behaviour (Fig. S4). Similarly, when we use the Wang–Frenkel potential[89] to model bead–bead non-bonded contacts, which significantly reduces the range of strong interactions (Fig. S1B pink curve), we find that just a minor increase of ε_S to values $\geq 6\,k_B$T is needed to bring condensates from a liquid-like state into the ageing regime (Fig. S6). If we assume that a standard protein diffusion coefficient of an intrinsically disordered protein within a phase-separated condensate is of the order of $\sim 1\,\mu m^2/s$ (Ref.[9]), we can estimate that the average time for a single protein to diffuse a typical distance within a condensate (i.e., 5 μm) is about 4 s. Hence, a protein diffusion deceleration of about 2–3 orders of magnitude, as the one we found in our simulations (Fig. 1B), would imply that proteins within aged condensates would require from 5 min to 1 h to migrate the same distance that takes them seconds inside a liquid-like droplet[35]. These relative timescales extracted from our simulations are consistent with the observed behaviour in time maturation experiments and FRAP recovery experiments applied to multiple aged condensates[23,34,65].

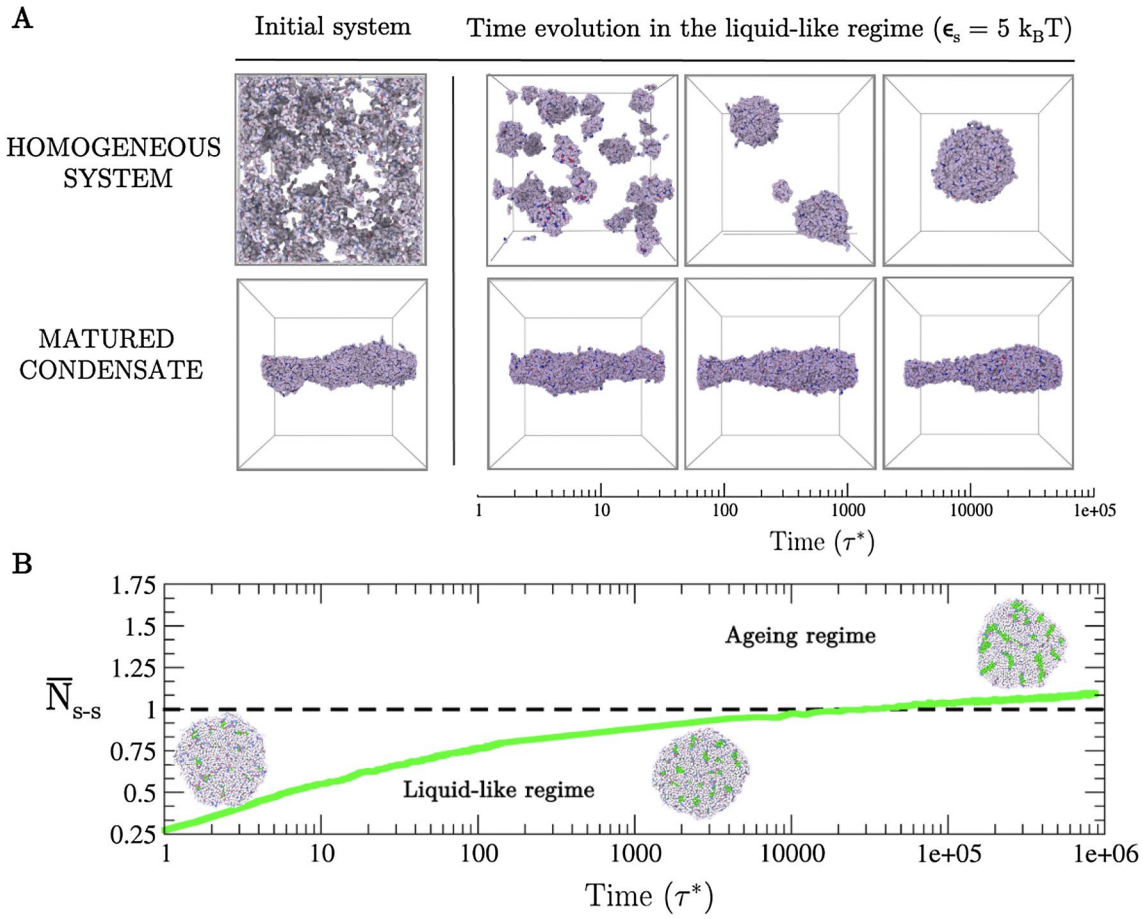

Figure 2. (**A**) Thermal hysteresis of the condensates probed via coarse-grained protein simulations. (Top panel) Time-evolution starting from an homogeneous system where inter-protein interactions are moderate (i.e., $\varepsilon_S = 5k_BT; \varepsilon_D = 0.5k_BT$). (Bottom panel) Time evolution at the same conditions above, although starting from a matured condensate that was formed under ageing regime conditions (i.e., strong inter-protein interactions of $\varepsilon_S = 6.6k_BT$). Note that in our model, temperature T is proportional to $\frac{1}{\varepsilon_{D(S)}}$. (**B**) Number of strong interactions as a function of time within a preformed spherical condensate ($\overline{N}_{s-s}$) normalised by the typical strong contact threshold (horizontal dashed line) that induces ageing behaviour of protein condensates at those conditions (i.e., number of strong interactions per condensate volume found at the cross-over of the blue curve with the kinetic threshold shown in Fig. 1B). Snapshots of the condensate shape as a function of time are shown. Protein segments that do not participate in strengthen contacts are depicted in grey, while those involved in clusters of stronger interactions are coloured in green. The protein interaction strength of this simulation was set to $\varepsilon_S = 6.6k_BT$, the same set value for the condensates shown in the bottom left panel of Fig. 1B.

We also study the thermal hysteresis of matured condensates. To that end, we set a protein interaction strength that enables liquid-liquid phase separation at T = 300 K ($\varepsilon_S = 5\,k_BT$; Top panel in Fig. 2A). From the initial homogeneous system, proteins nucleate several small spherical droplets that grow and coalesce, eventually yielding a single spherical larger condensate (i.e., the global free energy minimum in the liquid-like regime). By starting from the same homogeneous system, we then increase the interaction strength among proteins to $\varepsilon_S = 6.6\,k_BT$ (ageing regime) in order to promote the formation of stronger longer-lived interactions. As expected from Fig. 1B, we observe the emergence of an amorphous elongated kinetically-arrested condensate (Fig. 2A (Left bottom panel)). Interestingly, when reducing the protein interaction strength back to the previous value ($\varepsilon_S = 5\,k_BT$), thereby mimicking the heating of an aged condensate, the aggregate remains in the dynamically arrested configuration, instead of relaxing into a spherical liquid-like condensate as in Fig. 2A (Top panel). Please note that since we are working with reduced units (i.e. $T^* = k_BT/\varepsilon$), reducing the protein interaction strength in our model is equivalent to increasing the actual temperature T. Accordingly, the system displays hysteresis behaviour. The observed hysteresis is a consequence of the free energy barrier needed to break the small clusters of strong binding domains that are gradually formed over time within aged condensates. We note that hysteresis will widely depend on the associated binding energy of the strongly binding protein segments, and on the thermodynamic pathway. Therefore, subtle variations on these magnitudes (i.e., in our model ε_S and ε_D) can significantly impact the degree of hysteresis[90]. For the sequence patterning with stickers distributed over the first half of the chain (Fig. S1A (Bottom)), thermal hysteresis can be observed within a similar range of temperatures (Fig. S5). However, when stronger interactions are modelled through the Wang–Frenkel potential[89] but maintaining the

original sequence patterning (Fig. 1A), hysteresis is only observed until $\varepsilon_S \sim 5.8\,k_BT$ (Fig. S7). These results highlight how small differences in sequence patterning (Fig. S4) or intermolecular interaction range (Fig. S7) can lead to moderate variations in the thermodynamic pathway and conditions arresting condensate dynamics and leading to thermal hysteresis. Nevertheless, we have also verified for all our simulations that when heating up the matured condensate even further (by changing ε_S from $6.6\,k_BT$ to $3.5\,k_BT$ and ε_D values correspondingly), full dissolution occurs in all cases. Such behaviour correctly recapitulates the moderate thermal hysteresis of hydrogels sustained by reversible fibrils[74–76] or the salt resistance hysteresis observed in different RNA-binding proteins such as FUS[49] or hnRNPA1[65,79].

Strikingly, we also find that when stronger inter-protein interactions emerge inside of already formed spherical droplets, instead of during the condensate nucleation and growth stages, the droplets only experience a modest shape deformation over time (Fig. 2B). To interrogate this behaviour, we estimate the average number of strong inter-protein contacts required to drive the condensate out of the liquid-like regime to a kinetically arrested state (i.e., strong contacts per condensate volume at the cross-over between liquid-like and ageing regimes in Fig. 1B). We then assess the number of strong inter-protein interactions as a function of time (green curve and green spheres in Fig. 2B, further details on these calculations are provided in Section *SIC*), and observe that even after crossing the threshold number of strong inter-protein contacts needed to trigger ageing behaviour (horizontal dashed line), condensates still remain roughly spherical. Once the droplet reaches a given number of strong inter-protein contacts per unit of volume, characteristic of a kinetically arrested condensate (which can be inferred from those shown in Fig. 1B), it becomes very unlikely that the condensate can undergo noticeable reshaping. Along the maturation pathway, a spherical liquid-like condensate is expected to mainly sample configurations that conserve the shape of the condensate until strong binding inter-protein domains find each other and associate into long-lived local clusters, which in turn, would decrease the mobility of that region, thus constraining even more the configurational sampling of the condensate to roughly spherical shapes. Such behaviour should be gradually accentuated by the lower diffusion of the large amount of proteins that increasingly engage over time in long-lived interactions. Although such proteins can rearrange locally to maximise their enthalpic gain via strong inter-protein bonds, they cannot diffuse sufficiently to yield alternative condensate arrangements of potentially lower free energy. In that respect, our results are consistent with the widely recognised asphericity as a consequence of condensate maturation[35,49], as long as the origin of such asphericity is mainly due to non-ergodic droplet coalescence, as discussed in the following section. Fusion of small protein clusters to matured condensates is expected to significantly contribute to the formation of aspherical condensates as shown in Fig. 1B (Bottom Right panel). Moreover, impaired exchange of molecules between condensates and their surroundings, as observed in different multivalent proteins[60,91], can lead to the emergence of irregular morphologies. In that respect, mean-field model simulations[92–94], minimal CG models[95–97] and high-resolution sequence-dependent force fields[98–105] has been shown to be extremely useful in providing thermodynamic guidance on phase-separation and hardening phenomena[106,107].

Kinetic interplay between droplet maturation and coalescence. Next, we investigate the kinetic competition between condensate maturation and growth due to droplet coalescence. Accordingly, we evaluate the time required for complete coalescence, which we term coalescence time (τ_c), of two spherical droplets (in tangent contact) into a single spherical condensate. We calculate the coalescence time for pairs of droplets of different sizes (from 50 to 500 proteins each) and for distinct values of strong inter-protein binding strength (Fig. 3). We observe that weak inter-protein interaction strengths allow complete fusion of the two initial droplets into a single larger spherical droplet (filled squares; liquid-like regime). Moreover, small droplets fuse considerably quicker than large condensates (i.e., 50-protein droplets fuse up to four times faster than 500-protein condensates at $\varepsilon_S = 5k_BT$). However, as the inter-protein interaction strength increases—for instance due to the emergence of solid-like nuclei sustained by 'sticker–sticker' enhanced binding interactions—and/or the coalescence time slows down, the initial condensate pairs are no longer able to rearrange into a single spherical droplet on the accessible simulation timescales due to condensate maturation (empty squares, ageing regime; please note that these symbols depict the (arbitrary) maximum simulated time in which tangent droplets were not able to either achieve complete coalescence or show strong trends of the formation of a single spherical shape.).

To highlight how the interplay between coalescence time and protein interaction strength commits condensates to either the liquid-like or the ageing regime, we define a border that divides both scenarios (blue curve in Fig. 3) and that we derive from the intersection between the time-evolution diffusion coefficients and the kinetic threshold (horizontal black dashed line) shown in Fig. 1B (Left panel). Provided that the kinetic threshold defined in Fig. 1B is reasonable, this border allow us to distinguish the liquid-like regime from the ageing scenario. At weak inter-protein interactions, coalescence needs to be extremely slow for condensates to enter into the ageing regime before complete fusion takes place, while at strong inter-protein interactions even fast coalescence times for very small droplets may result in aged aspherical condensates. Remarkably, we find that this border—inferred from the time-evolution of bulk protein diffusivities and condensate shapes shown in Fig. 1B, as well as from the time-dependence behaviour of condensate density (Fig. S2) and protein intermolecular interactions (Fig. S3)—effectively discriminates the behaviour of kinetically trapped condensates (empty squares) from those that can equilibrate into spherical droplets (filled squares) in our coalescence simulations (Fig. 3). Moreover, Figs. S2 and S3 reveal that binding strengths greater than $\varepsilon_S = 5\,k_BT$ lead to bulk condensate equilibration timescales at least one order of magnitude slower than at $\varepsilon_S = 5\,k_BT$ ($< 10^5\,\tau^*$ units); for the strongest interactions (i.e., $\varepsilon_S = 5.5\,k_BT$ and $6.6\,k_BT$), the equilibration timescales can be several orders of magnitude larger than those at $\varepsilon_S = 5\,k_BT$ (Fig. S3).

These results further demonstrate how droplet shape can be critically modulated by the competition between two distinct timescales: coalescence time and maturation rate. This behaviour is particularly well exemplified

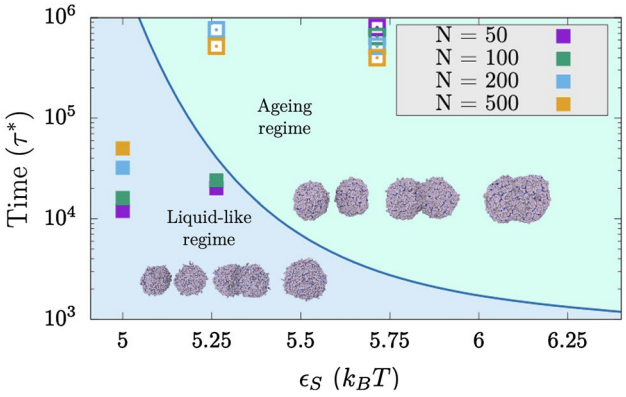

Figure 3. Competition between droplet coalescence time and maturation rate as a function of strong inter-protein interactions (ε_S) for different droplet sizes. Blue curve, termed 'border', depicts the lapse of time before proteins enter into the ageing (kinetically-trapped) regime due to the emergence of long-lived contacts. The blue curve is a kinetic line that is defined as the intersection of the different diffusion curves and the horizontal kinetic threshold shown in Fig. 1B (Left panel). Filled squares represent the time required for two spherical tangent droplets of a given size to fuse into a single spherical condensate, while empty squares depict the (arbitrary) maximum simulated time for tangent droplets that did not achieve complete coalescence or shown strong trends of the formation of a single spherical condensate. Snapshots of the typical time-evolution of coalescing droplets in both regimes at $\varepsilon_S = 5.25 k_B$T are included for droplet sizes of 100 (liquid-like regime) and 200 proteins (ageing regime).

by the simulations at inter-protein interaction strengths just sufficiently high to give rise to arrested glass-like behaviour (i.e., $\varepsilon_S = 5.25\,k_B$T). In this case, for the smallest droplet sizes (50 and 100 proteins per droplet, purple and green squares respectively in Fig. 3), the time required for droplet fusion and minimisation of the system's free energy (i.e., forming a spherical condensate) is shorter than the maturation time (i.e., the formation of long-lived interactions that cause the system to become kinetically trapped). However, for larger droplet sizes (i.e., those containing 200 and 500 proteins), the condensate (both tangent droplets) becomes kinetically arrested before achieving a spherical arrangement. On the other hand, moderate inter-protein interactions permit the complete coalescence of all tested condensate sizes into spherical droplets ($\varepsilon_S = 5\,k_B$T), while stronger interactions (i.e., $\varepsilon_S = 5.75\,k_B$T) do not yield complete fusion of even the smallest tested droplets (Fig. 3). We note that the quantitative absolute values of the kinetic and thermodynamic magnitudes measured in our simulations are determined by the specific features of our models and the implicit treatment of the solvent. Nevertheless, the qualitative relative trends that we observe for these magnitudes (i.e., D or ρ) over time, and the interplay between droplet fusion rate, protein binding strength and protein mobility (measured in Fig. 3) are expected to hold. For instance, having implicit solvent overestimates protein self-diffusion within the condensates, but also increases the droplet fusion rate of the two tangent droplets. In addition, while protein diffusion coefficient are likely overestimated, we are neglecting the small free energy barriers associated to the emergence of strong-binding domains that are accomplished through disorder-to-order structural transitions[108]. Overall, our simulations highlight how small variations in the binding energy between protein domains can crucially modulate the liquid-like behaviour, and ultimately the shape of biomolecular condensates.

Based on Figs. 2 and 3, we argue that condensate asphericity seems to be fundamentally determined by fusion events of kinetically arrested droplets rather than from maturation of preformed spherical condensates. Moreover, we note that different patterning[95] of strong-binding domains along the protein sequence (Figs. S4 and S5), does not show a qualitatively distinct behaviour to that of Fig. 2 in terms of shape evolution along condensate maturation[39].

Comparing the strength of inter-protein interactions among disordered versus ordered peptides. In this section, we quantify the change in the strength of inter-protein interactions due to the formation of inter-protein β-sheets, to determine if such change may be consistent with the dynamical arrest we describe in our coarse-grained simulations. We are particularly interested in the formation of inter-protein β-sheets because they can emerge spontaneously and intrinsically, i.e., without requiring changes in the chemistry of the system or the environmental conditions. Interestingly, the intrinsically disordered regions of various phase-separating naturally occurring proteins—including fused in sarcoma (FUS)[75], TAR DNA-binding Protein of 43 kDa (TDP-43)[76], heterogeneous nuclear ribonucleoprotein A1 (hnRNPA1)[74,79,80], and nucleoprotein of 98 kDa (NUP-98)[74,109]—which form hydrogels over time[73,110,111], contain short regions termed Low-complexity Aromatic-Rich Kinked Segments (LARKS) that are prone to form such inter-protein β-sheets[82]. When multiple LARKS meet at the high concentrations found inside condensates, they can assemble into ordered arrays of inter-protein β-sheet structures that stick to one another strongly via π–π bonds and hydrogen bonding between backbone atoms that may lead to gradual solidification of, otherwise, liquid-like condensates[72,74,75,77,87,112]. Importantly, hundreds of protein sequences capable of such disorder-to-order conformational transitions, and concomitant enhancement of intermolecular binding strengths, have been identified in the human genome[74].

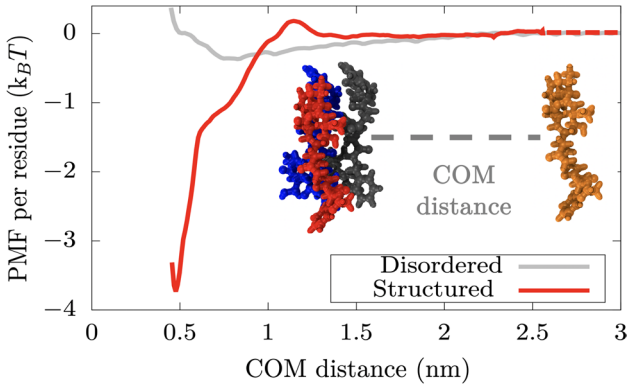

Figure 4. Atomistic potential-of-mean-force (PMF) dissociation curve of an 8-amino acid segment (PDB code: 6BZM) of NUP-98 protein from a β-sheet structure of 4 peptides (of the same sequence) as a function of the center of mass distance (COM) using the a99SB-*disp* force field[116]. Red curve depicts the interaction strength among peptides with a well-defined folded structure, kinked β-sheet structure, while grey curve represents the interaction strength among the same segments but when they are disordered. The binding interaction strength difference between disordered and ordered peptides differs by almost an order of magnitude. The same calculations performed using the CHARM36m force field[117] are shown in Fig. S9, where the obtained difference in binding strength between disordered and structured peptides is of the same order.

As a case study, we focus on the NUP-98 protein—an aggregation-prone protein that phase separates in vitro under selective conditions and can form hydrogels under others[113,114]. We start by estimating the binding strength among four interacting NUP-98 LARKS-containing peptides by means of Umbrella Sampling Molecular Dynamics simulations[115] in explicit solvent and ions under two distinct scenarios: (1) when all the peptides are fully disordered, and (2) when peptides form the inter-peptide cross-β-sheet motif resolved crystallographically (PDB code: 6BZM)[74]. From these simulations (using the a99SB-*disp* force field[116]), we compute the potential of mean force (PMF) as a function of the centre-of-mass (COM) distance between one single peptide—which we gradually force to dissociate from the other segments—and the other three segments (simulation details are described in section *SII* of the Supplementary Information). For the scenario when LARKS are treated as fully disordered, we allow peptides to freely sample their conformational space (only fixing the position (in the appropriate direction) of the closest atom to the peptide COM of the structured four-peptide array; see SI for further details). In the second scenario, where we quantify the interactions among ordered LARKS, we constrain the peptides to retain their crystal β-sheet structure[74].

Our simulations reveal that the interaction strength between disordered unconstrained peptides is sufficiently weak (i.e., $< 0.5k_BT$ per residue) that, at room temperature, thermal fluctuations would frequently break and reform such inter-protein interactions, consistent with the formation of liquid-like condensates (Fig. 4, grey curve). More interestingly, when the peptides assemble into constrained inter-peptide cross-β-sheet structures, the strength of their interactions increases by almost an order of magnitude (i.e., to approximately $4k_BT$ per residue, red curve). To verify that our conclusions on the relative difference between disordered and structured binding are not model dependent, we also compute the PMF dissociation curve using the CHARMM36m force field[117]. As shown in Fig. S9 of the SI, a ten fold difference between both peptide dissociation curves is also obtained in agreement with our calculations using the a99SB-*disp* force field[116] (Fig. 4). We note, however, that the exact magnitude of this increase may be slightly overestimated by the constraints we have used to enforce the stability of the β-sheet structures (which likely contribute to increase the free energy of the β-sheet structure respect to the random coil, and therefore, the global minimum depth respect to the fully dissociated state). Nevertheless, these results, together with our coarse-grained simulations, suggest that an enhancement of inter-protein interactions may occur due to the formation of inter-peptide LARKS β-sheets, sufficient to sustain the formation of gels or aged solid-like aggregates. Importantly, the strength of structured LARKS–LARKS interactions remain sufficiently weak that they can still be considered thermolabile. Our results are also consistent with experiments reporting that LARKS-containing proteins form reversible hydrogels that can be easily dissolved with heat[74–76]. A significant increase in the interaction strength after a disorder-to-order transition has been reported previously for the $A\beta$1–42 system[77]. However, in the case of $A\beta$1–42, the observed increase was much larger, consistent with amyloid fibers being thermostable[118,119]. Our previous coarse-grained simulations may reasonably describe the gradual rigidification that condensates can display due to the emergence of inter-protein β-sheet clusters (Fig. 4). Still, the free energy penalty associated to the structural transition, or more critically, the variation in binding strength after the cross-β-sheet formation is only approximated within our approach. Nevertheless, when we employ a time-dependent and spatially-dependent Hamiltonian coupled to a local order parameter[97] that enables variations in the binding strength among LARKS as a function of their local environment, we find consistent results of condensate maturation[120] than those using a static model like the one in the present work (Figs. 3 and 4 of Ref.[120]). Our simulations in Ref.[120] reveal that a static model reasonably describes ageing due to strengthening of inter-protein interactions when the abundance of strongly-binding domains along the protein sequence is relatively low (Fig. 1A). Using a static model is necessary when dealing with extremely long system

relaxation timescales and low protein self-diffusion as in the present work. A static model with low abundance of strongly-binding domains along the protein sequence can still adequately balance the β-sheet transition timescale (typically of the order of hundreds of nanoseconds[121–123]) and the protein self-diffusion timescale (of the order of hundreds of milliseconds[9]); thus, enabling the gradual rigidification of phase-separated condensates after protein aggregation[23,34,49,65] as recently observed for different DNA- and RNA-binding proteins[74,124,125].

Conclusions

In this work, we investigate the impact of enhanced inter-protein interactions in the modulation of the kinetic and thermodynamic properties of ageing biomolecular condensates. Our coarse-grained protein model shows that condensates remain liquid-like when proteins bind to one another weakly (i.e., $< 1\ k_BT$), but strengthening of inter-protein interactions (i.e., $> 5\ k_BT$ per residue) gradually slows down the mobility of proteins over time, leading to progressive rigidification/maturation of the condensates[23,49]. We also observe that aged condensates exhibit a significant degree of hysteresis: once long-lived ordered–ordered interactions are established, amorphous condensates become heat resistant up to moderate temperatures close to the critical conditions for phase separation[126]. Consistently, our atomistic simulations, reveal that formation of inter-peptide β-sheets, such as those that may form within the LARKS regions of NUP-98[74,125], and similarly in FUS, TDP-43 or hnRNPA1 among other proteins[23,34,74,127], can increase the interaction strength between these segments significantly. Such strong binding variation may contribute to rationalise the physicochemical and molecular factors behind the intricate process of pathological maturation and formation of amorphous phase-separated condensates observed in LARKS-containing proteins such as FUS[49], hnRNPA1[23], TDP-43[124], or NUP-98[74,109].

We also illustrate how the coupled effects of the decay in protein mobility, the timescale for the emergence of long-lived interactions, droplet coalescence times, and droplet size, crucially govern the shape and material properties of the condensates. When strong inter-protein binding occurs faster than droplet coalescence, the resulting condensates are non-spherical[128,129]. However, when the strengthening of protein interactions emerge after condensate formation (i.e., once a spherical droplet is already formed), the condensate only experiences a very slight deformation remaining mostly spherical. The time required for two separate tangent droplets to fuse and rearrange into a single spherical condensate depends on both, the initial size of the droplets that are attempting to fuse, and the strength of inter-protein interactions. In small condensates, where the rearrangement time is shorter than the timescale in which proteins lose their mobility due to clustering of structured motifs, condensates are mostly spherical but can eventually become kinetically arrested. In contrast, in larger droplets, where coalescence times are longer, the loss of protein mobility occurs faster than the time required for the condensate to rearrange, and therefore, protein aggregates become kinetically trapped in non-spherical or partially-fused states. Taken together, our results shed light on how local strengthening of inter-protein interactions—for instance due to formation of inter-protein β-sheets[74–76,79,80], establishment of post-translational modifications[81], or changes in salt conditions[26]—may impact the mesoscopic phase behaviour of biomolecular condensates, and suggest a mechanism for the emergence of aspherical droplets over time.

Received: 8 October 2021; Accepted: 7 February 2022
Published online: 15 March 2022

References

1. Sear, R. P. The cytoplasm of living cells: A functional mixture of thousands of components. *J. Phys. Condens. Matter* **17**, S3587–S3595 (2005).
2. Hyman, A. A., Weber, C. A. & Jülicher, F. Liquid–liquid phase separation in biology. *Annu. Rev. Cell Dev. Biol.* **30**, 39–58. https://doi.org/10.1146/annurev-cellbio-100913-013325 (2014).
3. Alberti, S. Phase separation in biology. *Curr. Biol.* **27**, R1097–R1102. https://doi.org/10.1016/j.cub.2017.08.069 (2017).
4. Shin, Y. & Brangwynne, C. P. Liquid phase condensation in cell physiology and disease. *Science* **357**, eaaf4382 (2017).
5. Alberts, B. *Molecular Biology of the Cell* 6th edn. (Garland Science, Taylor and Francis Group, New York, NY, 2015).
6. Hyman, A. A. & Simons, K. Beyond oil and water-phase transitions in cells. *Science* **337**, 1047–1049 (2012).
7. Banani, S. F., Lee, H. O., Hyman, A. A. & Rosen, M. K. Biomolecular condensates: Organizers of cellular biochemistry. *Nat. Rev. Mol. Cell Biol.* **18**, 285–298. https://doi.org/10.1038/nrm.2017.7 (2017).
8. Lyon, A. S., Peeples, W. B. & Rosen, M. K. A framework for understanding the functions of biomolecular condensates across scales. *Nat. Rev. Mol. Cell Biol.*https://doi.org/10.1038/s41580-020-00303-z *(2020).*
9. Strom, A. R. *et al.* Phase separation drives heterochromatin domain formation. *Nature* **547**, 241–245. https://doi.org/10.1038/nature22989 (2017).
10. Larson, A. G. *et al.* Liquid droplet formation by HP1α suggests a role for phase separation in heterochromatin. *Nature* **547**, 236–240. https://doi.org/10.1038/nature22822 (2017).
11. Sabari, B. R., Dall'Agnese, A. & Young, R. A. Biomolecular condensates in the nucleus. *Trends Biochem. Sci.* **45**, 961–977. https://doi.org/10.1016/j.tibs.2020.06.007 (2020).
12. Strom, A. R. & Brangwynne, C. P. The liquid nucleome—phase transitions in the nucleus at a glance. *J. Cell Sci.*https://doi.org/10.1242/jcs.235093 *(2019).*
13. Brangwynne, C. P. *et al.* Germline p granules are liquid droplets that localize by controlled dissolution/condensation. *Science* **324**, 1729–1732. https://doi.org/10.1126/science.1172046 (2009).
14. Brangwynne, C. P., Mitchison, T. J. & Hyman, A. A. Active liquid-like behavior of nucleoli determines their size and shape in *Xenopus laevis* oocytes. *Proc. Natl. Acad. Sci.* **108**, 4334–4339. https://doi.org/10.1073/pnas.1017150108 (2011).
15. Feric, M. *et al.* Coexisting liquid phases underlie nucleolar subcompartments. *Cell* **165**, 1686–1697. https://doi.org/10.1016/j.cell.2016.04.047 (2016).
16. Berry, J., Weber, S. C., Vaidya, N., Haataja, M. & Brangwynne, C. P. RNA transcription modulates phase transition-driven nuclear body assembly. *Proc. Natl. Acad. Sci.* **112**, E5237–E5245. https://doi.org/10.1073/pnas.1509317112 (2015).
17. Caragine, C. M., Haley, S. C. & Zidovska, A. Nucleolar dynamics and interactions with nucleoplasm in living cells. *eLife* **8**, e47533. https://doi.org/10.7554/eLife.47533 (2019).

18. Mitrea, D. M. *et al.* Nucleophosmin integrates within the nucleolus via multi-modal interactions with proteins displaying R-rich linear motifs and rRNA. *eLife* **5**, e13571. https://doi.org/10.7554/eLife.13571 (2016).
19. Weber, S. C. & Brangwynne, C. P. Inverse size scaling of the nucleolus by a concentration-dependent phase transition. *Curr. Biol. CB* **25**, 641–646. https://doi.org/10.1016/j.cub.2015.01.012 (2015).
20. Platani, M., Goldberg, I., Swedlow, J. R. & Lamond, A. I. In vivo analysis of Cajal body movement, separation, and joining in live human cells. *J. Cell Biol.* **151**, 1561–1574. https://doi.org/10.1083/jcb.151.7.1561 (2000).
21. Handwerger, K. E., Cordero, J. A. & Gall, J. G. Cajal bodies, nucleoli, and speckles in the *Xenopus* oocyte nucleus have a low-density, sponge-like structure. *Mol. Biol. Cell* **16**, 202–211. https://doi.org/10.1091/mbc.e04-08-0742 (2005).
22. Courchaine, E. M., Lu, A. & Neugebauer, K. M. Droplet organelles?. *EMBO J.* **35**, 1603–1612. https://doi.org/10.15252/embj.201593517 (2016).
23. Molliex, A. *et al.* Phase separation by low complexity domains promotes stress granule assembly and drives pathological fibrillization. *Cell* **163**, 123–133. https://doi.org/10.1016/j.cell.2015.09.015 (2015).
24. Ladouceur, A.-M. *et al.* Clusters of bacterial RNA polymerase are biomolecular condensates that assemble through liquid–liquid phase separation. *Proc. Natl. Acad. Sci.* **117**, 18540–18549. https://doi.org/10.1073/pnas.2005019117 (2020).
25. Nettels, D. *et al.* Single-molecule spectroscopy of the temperature-induced collapse of unfolded proteins. *Proc. Natl. Acad. Sci.* **106**, 20740–20745 (2009).
26. Krainer, G. *et al.* Reentrant liquid condensate phase of proteins is stabilized by hydrophobic and non-ionic interactions. *Nat. Commun.* **12**, 1–14 (2021).
27. Mitrea, D. M. & Kriwacki, R. W. Phase separation in biology; functional organization of a higher order. *Cell Commun. Signal.* **14**, 1–20 (2016).
28. Riback, J. A. *et al.* Composition-dependent thermodynamics of intracellular phase separation. *Nature* **581**, 209–214 (2020).
29. Alberti, S. & Dormann, D. Liquid–liquid phase separation in disease. *Annu. Rev. Genet.* **53**, 171–194. https://doi.org/10.1146/annurev-genet-112618-043527 (2019) (**PMID: 31430179**).
30. Alberti, S. & Hyman, A. A. Are aberrant phase transitions a driver of cellular aging?. *BioEssays* **38**, 959–968 (2016).
31. Shin, Y. & Brangwynne, C. P. Liquid phase condensation in cell physiology and disease. *Science*https://doi.org/10.1126/science.aaf4382 *(2017).*
32. Babinchak, W. M. & Surewicz, W. K. Liquid–liquid phase separation and its mechanistic role in pathological protein aggregation. *J. Mol. Biol.* **432**, 1910–1925. https://doi.org/10.1016/j.jmb.2020.03.004 (2020).
33. Nedelsky, N. B. & Taylor, J. P. Bridging biophysics and neurology: Aberrant phase transitions in neurodegenerative disease. *Nat. Rev. Neurol.* **15**, 272–286. https://doi.org/10.1038/s41582-019-0157-5 (2019).
34. Patel, A. *et al.* A liquid-to-solid phase transition of the ALS protein FUS accelerated by disease mutation. *Cell* **162**, 1066–1077. https://doi.org/10.1016/j.cell.2015.07.047 (2015).
35. Ray, S. *et al.*α-Synuclein aggregation nucleates through liquid–liquid phase separation. *Nat. Chem.* **12**, 705–716. https://doi.org/10.1038/s41557-020-0465-9 (2020).
36. Wegmann, S. *et al.* Tau protein liquid–liquid phase separation can initiate tau aggregation. *EMBO J.*https://doi.org/10.15252/embj.201798049 *(2018).*
37. Spannl, S., Tereshchenko, M., Mastromarco, G. J., Ihn, S. J. & Lee, H. O. Biomolecular condensates in neurodegeneration and cancer. *Traffic* **20**, 890–911 (2019).
38. Pytowski, L., Lee, C. F., Foley, A. C., Vaux, D. J. & Jean, L. Liquid–liquid phase separation of type II diabetes-associated IAPP initiates hydrogelation and aggregation. *Proc. Natl. Acad. Sci.* **117**, 12050. https://doi.org/10.1073/pnas.1916716117 (2020).
39. Portz, B., Lee, B. L. & Shorter, J. FUS and TDP-43 phases in health and disease. *Trends Biochem. Sci.* **46**, 550–563 (2021).
40. Qamar, S. *et al.* FUS phase separation is modulated by a molecular chaperone and methylation of arginine cation-π interactions. *Cell* **173**, 720–734. https://doi.org/10.1016/j.cell.2018.03.056 (2018).
41. Brangwynne, C. P., Mitchison, T. J. & Hyman, A. A. Active liquid-like behavior of nucleoli determines their size and shape in *Xenopus laevis* oocytes. *Proc. Natl. Acad. Sci.* **108**, 4334–4339 (2011).
42. Riback, J. A. & Brangwynne, C. P. Can phase separation buffer cellular noise?. *Science* **367**, 364–365. https://doi.org/10.1126/science.aba0446 (2020).
43. Larson, A. G. & Narlikar, G. J. The role of phase separation in heterochromatin formation, function, and regulation. *Biochemistry*https://doi.org/10.1021/acs.biochem.8b00401 *(2018).*
44. Mir, M., Bickmore, W., Furlong, E. E. M. & Narlikar, G. Chromatin topology, condensates and gene regulation: Shifting paradigms or just a phase?. *Development*https://doi.org/10.1242/dev.182766 *(2019).*
45. Laflamme, G. & Mekhail, K. Biomolecular condensates as arbiters of biochemical reactions inside the nucleus. *Commun. Biol.* **3**, 773. https://doi.org/10.1038/s42003-020-01517-9 (2020).
46. Yoo, H., Triandafillou, C. & Drummond, D. A. Cellular sensing by phase separation: Using the process, not just the products. *J. Biol. Chem.* **294**, 7151–7159. https://doi.org/10.1074/jbc.TM118.001191 (2019).
47. Arrasate, M., Mitra, S., Schweitzer, E. S., Segal, M. R. & Finkbeiner, S. Inclusion body formation reduces levels of mutant huntingtin and the risk of neuronal death. *Nature* **431**, 805–810. https://doi.org/10.1038/nature02998 (2004).
48. Fare, C. M., Villani, A., Drake, L. E. & Shorter, J. Higher-order organization of biomolecular condensates. *Open Biol.* **11**, 210137 (2021).
49. Jawerth, L. *et al.* Protein condensates as aging Maxwell fluids. *Science* **370**, 1317–1323 (2020).
50. Mathieu, C., Pappu, R. V. & Taylor, J. P. Beyond aggregation: Pathological phase transitions in neurodegenerative disease. *Science* **370**, 56–60 (2020).
51. Nakamura, H., DeRose, R. & Inoue, T. Harnessing biomolecular condensates in living cells. *J. Biochem.* **166**, 13–27 (2019).
52. Alberti, S. & Hyman, A. A. Biomolecular condensates at the nexus of cellular stress, protein aggregation disease and ageing. *Nat. Rev. Mol. Cell Biol.* **22**, 1–18 (2021).
53. Shen, Y. *et al.* Biomolecular condensates undergo a generic shear-mediated liquid-to-solid transition. *Nat. Nanotechnol.* **15**, 841–847 (2020).
54. Harmon, T. S., Holehouse, A. S., Rosen, M. K. & Pappu, R. V. Intrinsically disordered linkers determine the interplay between phase separation and gelation in multivalent proteins. *eLife*https://doi.org/10.7554/eLife.30294 *(2017).*
55. Bremer, A. *et al.* Deciphering how naturally occurring sequence features impact the phase behaviors of disordered prion-like domains. *bioRxiv* (2021).
56. Lu, T. & Spruijt, E. Multiphase complex coacervate droplets. *J. Am. Chem. Soc.* **142**, 2905–2914 (2020).
57. Boeynaems, S. *et al.* Protein phase separation: A new phase in cell biology. *Trends Cell Biol.*https://doi.org/10.1016/j.tcb.2018.02.004 *(2018).*
58. Sanders, D. W. *et al.* Competing protein–RNA interaction networks control multiphase intracellular organization. *Cell* **181**, 306–324 (2020).
59. Maharana, S. *et al.* RNA buffers the phase separation behavior of prion-like RNA binding proteins. *Science* **360**, 918–921 (2018).
60. Wang, J. *et al.* A molecular grammar governing the driving forces for phase separation of prion-like RNA binding proteins. *Cell* **174**, 688–699. https://doi.org/10.1016/j.cell.2018.06.006 (2018).
61. Sanulli, S. *et al.* Hp1 reshapes nucleosome core to promote phase separation of heterochromatin. *Nature* **575**, 390–394 (2019).
62. Gibson, B. A. *et al.* Organization of chromatin by intrinsic and regulated phase separation. *Cell* **179**, 470–484 (2019).

63. Wang, L. *et al.* Histone modifications regulate chromatin compartmentalization by contributing to a phase separation mechanism. *Mol. Cell* **76**, 646–659 (2019).
64. Shakya, A., Park, S., Rana, N. & King, J. T. Liquid–liquid phase separation of histone proteins in cells: Role in chromatin organization. *Biophys. J.* **118**, 753–764 (2020).
65. Lin, Y., Protter, D. S., Rosen, M. K. & Parker, R. Formation and maturation of phase-separated liquid droplets by RNA-binding proteins. *Mol. Cell* **60**, 208–219. https://doi.org/10.1016/j.molcel.2015.08.018 (2015).
66. Woodruff, J. B. *et al.* The centrosome is a selective condensate that nucleates microtubules by concentrating tubulin. *Cell* **169**, 1066-1077.e10. https://doi.org/10.1016/j.cell.2017.05.028 (2017).
67. Jang, S. *et al.* Phosphofructokinase relocalizes into subcellular compartments with liquid-like properties in vivo. *Biophys. J.*https://doi.org/10.1016/j.bpj.2020.08.002 *(2020).*
68. Nair, S. J. *et al.* Phase separation of ligand-activated enhancers licenses cooperative chromosomal enhancer assembly. *Nat. Struct. Mol. Biol.* **26**, 193–203. https://doi.org/10.1038/s41594-019-0190-5 (2019).
69. Franzmann, T. M. *et al.* Phase separation of a yeast prion protein promotes cellular fitness. *Science* **359**, eaao5654 (2018).
70. Dogra, P., Joshi, A., Majumdar, A. & Mukhopadhyay, S. Intermolecular charge-transfer modulates liquid–liquid phase separation and liquid-to-solid maturation of an intrinsically disordered pH-responsive domain. *J. Am. Chem. Soc.* **141**, 20380–20389 (2019).
71. Schisa, J. A. & Elaswad, M. T. An emerging role for post-translational modifications in regulating RNP condensates in the germ line. *Front. Mol. Biosci.* **8**, 230 (2021).
72. Ambadipudi, S., Biernat, J., Riedel, D., Mandelkow, E. & Zweckstetter, M. Liquid–liquid phase separation of the microtubule-binding repeats of the Alzheimer-related protein tau. *Nat. Commun.* **8**, 275. https://doi.org/10.1038/s41467-017-00480-0 (2017).
73. Murakami, T. *et al.* ALS/FTD mutation-induced phase transition of FUS liquid droplets and reversible hydrogels into irreversible hydrogels impairs RNP granule function. *Neuron* **88**, 678–690 (2015).
74. Hughes, M. P. *et al.* Atomic structures of low-complexity protein segments reveal kinked β sheets that assemble networks. *Science* **359**, 698. https://doi.org/10.1126/science.aan6398 (2018).
75. Luo, F. *et al.* Atomic structures of FUS LC domain segments reveal bases for reversible amyloid fibril formation. *Nat. Struct. Mol. Biol.* **25**, 341–346. https://doi.org/10.1038/s41594-018-0050-8 (2018).
76. Guenther, E. L. *et al.* Atomic structures of TDP-43 LCD segments and insights into reversible or pathogenic aggregation. *Nat. Struct. Mol. Biol.* **25**, 463–471. https://doi.org/10.1038/s41594-018-0064-2 (2018).
77. Šarić, A., Chebaro, Y. C., Knowles, T. P. & Frenkel, D. Crucial role of nonspecific interactions in amyloid nucleation. *Proc. Natl. Acad. Sci.* **111**, 17869–17874 (2014).
78. Murray, D. T. *et al.* Structure of FUS protein fibrils and its relevance to self-assembly and phase separation of low-complexity domains. *Cell* **171**, 615–627 (2017).
79. Gui, X. *et al.* Structural basis for reversible amyloids of hnRNPA1 elucidates their role in stress granule assembly. *Nat. Commun.* **10**, 1–12 (2019).
80. Sun, Y. *et al.* The nuclear localization sequence mediates hnRNPA1 amyloid fibril formation revealed by cryoEM structure. *Nat. Commun.* **11**, 1–8 (2020).
81. Rai, A. K., Chen, J.-X., Selbach, M. & Pelkmans, L. Kinase-controlled phase transition of membraneless organelles in mitosis. *Nature* **559**, 211–216 (2018).
82. Mendoza-Espinosa, P., García-González, V., Moreno, A., Castillo, R. & Mas-Oliva, J. Disorder-to-order conformational transitions in protein structure and its relationship to disease. *Mol. Cell. Biochem.* **330**, 105–120 (2009).
83. St George-Hyslop, P. *et al.* The physiological and pathological biophysics of phase separation and gelation of RNA binding proteins in amyotrophic lateral sclerosis and fronto-temporal lobar degeneration. *Brain Res.* **1693**, 11–23. https://doi.org/10.1016/j.brainres.2018.04.036 (2018) (**RNA Metabolism in Neurological Disease 2018.**).
84. Ferrolino, M. C., Mitrea, D. M., Michael, J. R. & Kriwacki, R. W. Compositional adaptability in NPM1-SURF6 scaffolding networks enabled by dynamic switching of phase separation mechanisms. *Nat. Commun.* **9**, 5064. https://doi.org/10.1038/s41467-018-07530-1 (2018).
85. Alberti, S., Gladfelter, A. & Mittag, T. Considerations and challenges in studying liquid–liquid phase separation and biomolecular condensates. *Cell* **176**, 419–434 (2019).
86. Tröster, A., Schmitz, F., Virnau, P. & Binder, K. Equilibrium between a droplet and surrounding vapor: A discussion of finite size effects. *J. Phys. Chem. B* **122**, 3407–3417 (2017).
87. Chuang, E., Hori, A. M., Hesketh, C. D. & Shorter, J. Amyloid assembly and disassembly. *J. Cell Sci.*https://doi.org/10.1242/jcs.189928 *(2018).*
88. Guo, L. & Shorter, J. It's raining liquids: RNA tunes viscoelasticity and dynamics of membraneless organelles. *Mol. Cell* **60**, 189–192 (2015).
89. Wang, X., Ramírez-Hinestrosa, S., Dobnikar, J. & Frenkel, D. The Lennard–Jones potential: When (not) to use it. *Phys. Chem. Chem. Phys.* **22**, 10624–10633 (2020).
90. Ow, S.-Y. & Dunstan, D. E. The effect of concentration, temperature and stirring on hen egg white lysozyme amyloid formation. *Soft Matter* **9**, 9692–9701 (2013).
91. Berry, J., Brangwynne, C. P. & Haataja, M. Physical principles of intracellular organization via active and passive phase transitions. *Rep. Prog. Phys.* **81**, 046601 (2018).
92. McCarty, J., Delaney, K. T., Danielsen, S. P., Fredrickson, G. H. & Shea, J.-E. Complete phase diagram for liquid–liquid phase separation of intrinsically disordered proteins. *J. Phys. Chem. Lett.* **10**, 1644–1652 (2019).
93. Weber, C. A., Zwicker, D., Jülicher, F. & Lee, C. F. Physics of active emulsions. *Rep. Prog. Phys.* **82**, 064601 (2019).
94. Lee, J., Popov, Y. O. & Fredrickson, G. H. Complex coacervation: A field theoretic simulation study of polyelectrolyte complexation ARTICLES YOU MAY BE INTERESTED IN. *J. Chem. Phys.* **128**, 224908. https://doi.org/10.1063/1.2936834 (2008).
95. Statt, A., Casademunt, H., Brangwynne, C. P. & Panagiotopoulos, A. Z. Model for disordered proteins with strongly sequence-dependent liquid phase behavior. Tech. Rep.
96. Blas, F., Ignacio Moreno-Ventas Bravo, A., Míguez, J., Piñeiro, M. & MacDowell, L. Vapor–liquid interfacial properties of rigid-linear Lennard–Jones chains. *J. Chem. Phys.* **137**, 084706 (2012).
97. Sanchez-Burgos, I., Joseph, J. A., Collepardo-Guevara, R. & Espinosa, J. R. Size conservation emerges spontaneously in biomolecular condensates formed by scaffolds and surfactant clients. *Sci. Rep.* **11**, 15241 (2021).
98. Tesei, G., Schulze, T. K., Crehuet, R. & Lindorff-Larsen, K. Accurate model of liquid–liquid phase behaviour of intrinsically-disordered proteins from optimization of single-chain properties. *bioRxiv* (2021).
99. Latham, A. P. & Zhang, B. Consistent force field captures homologue-resolved hp1 phase separation. *J. Chem. Theory Comput.* **17**, 3134–3144 (2021).
100. Latham, A. P. & Zhang, B. Unifying coarse-grained force fields for folded and disordered proteins. *Curr. Opin. Struct. Biol.* **72**, 63–70 (2022).
101. Dignon, G. L., Zheng, W., Kim, Y. C., Best, R. B. & Mittal, J. Sequence determinants of protein phase behavior from a coarse-grained model. *PLoS Comput. Biol.*https://doi.org/10.1371/journal.pcbi.1005941 *(2018).*
102. Joseph, A. J. *et al.* Physics-driven coarse-grained model for biomolecular phase separation with near-quantitative accuracy. *Nat. Comput. Sci.* in press (2021).

103. Garaizar, A. & Espinosa, J. R. Salt dependent phase behavior of intrinsically disordered proteins from a coarse-grained model with explicit water and ions. *J. Chem. Phys.* **155**, 125103 (2021).
104. Regy, R. M., Dignon, G. L., Zheng, W., Kim, Y. C. & Mittal, J. Sequence dependent phase separation of protein-polynucleotide mixtures elucidated using molecular simulations. *Nucl. Acids Res.* **48**, 12593–12603. https://doi.org/10.1093/nar/gkaa1099 (2020).
105. Tejedor, A. R., Garaizar, A., Ramírez, J. & Espinosa, J. R. RNA modulation of transport properties and stability in phase separated condensates. *Biophys. J.* **120**, 5169–5186 (2021).
106. Choi, J.-M., Hyman, A. A. & Pappu, R. V. Generalized models for bond percolation transitions of associative polymers. *Phys. Rev. E* **102**, 042403 (2020).
107. Sciortino, F., Bansil, R., Stanley, H. E. & Alstrøm, P. Interference of phase separation and gelation: A zeroth-order kinetic model. *Phys. Rev. E* **47**, 4615 (1993).
108. Alm, E. & Baker, D. Prediction of protein-folding mechanisms from free-energy landscapes derived from native structures. *Proc. Natl. Acad. Sci.* **96**, 11305–11310 (1999).
109. Milles, S. *et al.* Facilitated aggregation of FG nucleoporins under molecular crowding conditions. *EMBO Rep.* **14**, 178–183 (2013).
110. Kato, M. *et al.* Cell-free formation of RNA granules: Low complexity sequence domains form dynamic fibers within hydrogels. *Cell* **149**, 753–767 (2012).
111. Hennig, S. *et al.* Prion-like domains in RNA binding proteins are essential for building subnuclear paraspeckles. *J. Cell Biol.* **210**, 529–539 (2015).
112. Liu, C. *et al.* Out-of-register β-sheets suggest a pathway to toxic amyloid aggregates. *Proc. Natl. Acad. Sci.* **109**, 20913–20918. https://doi.org/10.1073/pnas.1218792109 (2012).
113. Schmidt, H. B. & Görlich, D. Nup98 FG domains from diverse species spontaneously phase-separate into particles with nuclear pore-like permselectivity. *Elife* **4**, e04251 (2015).
114. Lindt, J. v. *et al.* A generic approach for studying the kinetics of liquid–liquid phase separation under near-native conditions. *bioRxiv*https://doi.org/10.1101/563700 *(2019).*
115. Lemkul, J. A. & Bevan, D. R. Assessing the stability of Alzheimer's amyloid protofibrils using molecular dynamics. *J. Phys. Chem. B* **114**, 1652–1660. https://doi.org/10.1021/jp9110794 (2010).
116. Robustelli, P., Piana, S. & Shaw, D. E. Developing a molecular dynamics force field for both folded and disordered protein states. *Proc. Natl. Acad. Sci.* **115**, E4758–E4766 (2018).
117. Huang, J. *et al.* Charmm36m: An improved force field for folded and intrinsically disordered proteins. *Nat. Methods* **14**, 71–73. https://doi.org/10.1038/nmeth.4067 (2017).
118. Lu, Y., Lim, L. & Song, J. RRM domain of ALS/FTD-causing FUS characteristic of irreversible unfolding spontaneously self-assembles into amyloid fibrils. *Sci. Rep.* **7**, 1–14 (2017).
119. Ramírez-Alvarado, M., Merkel, J. S. & Regan, L. A systematic exploration of the influence of the protein stability on amyloid fibril formation in vitro. *Proc. Natl. Acad. Sci.* **97**, 8979–8984 (2000).
120. Garaizar, A. *et al.* Intermolecular reorganisation of single-component condensates during ageing promotes multiphase architectures. *bioRxiv*https://doi.org/10.1101/2021.10.09.463670 *(2021).*
121. Kathuria, S. V. *et al.* Minireview: Structural insights into early folding events using continuous-flow time-resolved small-angle x-ray scattering. *Biopolymers* **95**, 550–558 (2011).
122. Huang, J.J.-T., Larsen, R. W. & Chan, S. I. The interplay of turn formation and hydrophobic interactions on the early kinetic events in protein folding. *Chem. Commun.* **48**, 487–497 (2012).
123. Kubelka, J., Hofrichter, J. & Eaton, W. A. The protein folding 'speed limit'. *Curr. Opin. Struct. Biol.* **14**, 76–88 (2004).
124. Zhuo, X.-F. *et al.* Solid-state NMR reveals the structural transformation of the TDP-43 amyloidogenic region upon fibrillation. *J. Am. Chem. Soc.* **142**, 3412–3421 (2020).
125. Liang, Y., Franks, T. M., Marchetto, M. C., Gage, F. H. & Hetzer, M. W. Dynamic association of nup98 with the human genome. *PLoS Genet* **9**, e1003308 (2013).
126. Kato, M. *et al.* Cell-free formation of RNA granules: Low complexity sequence domains form dynamic fibers within hydrogels. *Cell* **149**, 753–767. https://doi.org/10.1016/j.cell.2012.04.017 (2012).
127. Xiang, S. *et al.* The LC domain of hnRNPA2 adopts similar conformations in hydrogel polymers, liquid-like droplets, and nuclei. *Cell* **163**, 829–839 (2015).
128. Linsenmeier, M. *et al.* Dynamic arrest and aging of biomolecular condensates are regulated by low-complexity domains, RNA and biochemical activity. *bioRxiv* (2021).
129. Hazra, M. K. & Levy, Y. Charge pattern affects the structure and dynamics of polyampholyte condensates. *Phys. Chem. Chem. Phys.* **22**, 19368–19375 (2020).

Acknowledgements

This project has received funding from the European Research Council (ERC) under the European Union Horizon 2020 research and innovation programme (Grant Agreement No 803326). J.R.E. acknowledges funding from the Oppenheimer Fellowship and from Emmanuel College Roger Ekins Research Fellowship. A.G. acknowledges funding from the EPRSC Doctoral Programme Training number EP/N509620/ and Winton Advanced program. J.A.J. is a Research Fellow at King's College. This work has been performed using resources provided by the Cambridge Tier-2 system operated by the University of Cambridge Research Computing Service (http://www.hpc.cam.ac.uk) funded by EPSRC Tier-2 capital Grant EP/P020259/1.

Author contributions

R.C.G. and J.R.E. conceived the project. A.G. and J.R.E. conducted the simulations. A.G. and J.R.E. analyzed the results. J.A.J. and R.C.G. contextualized the results. All the authors wrote the initial draft of the manuscript. All the authors reviewed and edited the manuscript.

Competing interests

The authors declare no competing interests.

Additional information

Supplementary Information The online version contains supplementary material available at https://doi.org/10.1038/s41598-022-08130-2.

Correspondence and requests for materials should be addressed to R.C.-G.

Reprints and permissions information is available at www.nature.com/reprints.

Publisher's note Springer Nature remains neutral with regard to jurisdictional claims in published maps and institutional affiliations.

Open Access This article is licensed under a Creative Commons Attribution 4.0 International License, which permits use, sharing, adaptation, distribution and reproduction in any medium or format, as long as you give appropriate credit to the original author(s) and the source, provide a link to the Creative Commons licence, and indicate if changes were made. The images or other third party material in this article are included in the article's Creative Commons licence, unless indicated otherwise in a credit line to the material. If material is not included in the article's Creative Commons licence and your intended use is not permitted by statutory regulation or exceeds the permitted use, you will need to obtain permission directly from the copyright holder. To view a copy of this licence, visit http://creativecommons.org/licenses/by/4.0/.

© The Author(s) 2022